Journal of Electroceramics, 14, 283–291, 2005

Impedance/Dielectric Spectroscopy of Electroceramics–Part 1: *Evaluation of Composite Models for Polycrystalline Ceramics*

N.J. KIDNER,[1] Z.J. HOMRIGHAUS,[1] B.J. INGRAM,[1] T.O. MASON[1] & E.J. GARBOCZI[2]

[1] *Department of Materials Science and Engineering and Materials Research Center, Northwestern University, Evanston, IL 60208, USA*
[2] *Materials and Construction Research, Building and Fire Research Laboratory, National Institute of Standards and Technology, Gaithersburg, MD 20899, USA*

Submitted October 21, 2003; Revised December 29, 2004; Accepted January 4, 2005

Abstract. In the microcrystalline regime, the electrical (impedance/dielectric) behavior of grain boundary-controlled electroceramics is well described by the "brick-layer model" (BLM). In the nanocrystalline regime, however, grain boundary layers can represent a significant volume fraction of the overall microstructure. Simple boundary-layer models no longer adequately describe the electrical properties of nanocrystalline ceramics. The present work describes the development of a pixel-based finite-difference approach to treat a "nested-cube model" (NCM), which is used to investigate the validity of existing models for describing the electrical properties of polycrystalline ceramics over the entire range of grain core vs. grain boundary volume fractions, from the nanocrystalline regime to the microcrystalline regime. The NCM is shown to agree closely with the Maxwell-Wagner effective medium theory.

Keywords: impedance, dielectric, effective medium, brick layer model, nested cube model

1. Introduction

The influence of grain boundaries on the point defect and related transport properties of ceramics has been well documented [1, 2]. The functionality of many technologically important electroceramics relies on electrical properties derived from their grain boundary-controlled behavior. For example, the electro-active and thermo-active responses of microcrystalline electroceramics (e.g., varistors and thermistors) derive from grain boundaries, whose properties differ significantly from those of the grain cores [3]

The reduction of grain size from the microcrystalline regime into the nanocrystalline regime is known to produce significant changes in the defect and transport properties of electroceramics [4]. Given the high surface-to-volume ratio in nanoceramics, grain boundaries are expected to exert a greater influence over the electrical/dielectric properties than in conventional microcrystalline ceramics. As a result, nanoceramics have potential for applications ranging from batteries to fuel cells, gas separation membranes, solar cells, etc. [5, 6]. To better understand the role of nanosized grains on the transport and dielectric properties of electroceramics, it is necessary to accurately model their electrical/dielectric properties as a function of grain size. Termed continuum models, since they replace the real microstructure with a microstructure that obeys the continuum Maxwell's equations, existing boundary layer models (see below) have several problems insofar as describing the electrical/dielectric response of nanoceramics is concerned. The first problem is that in the nanograin regime, boundary layers can represent a significant volume fraction of the overall microstructure. The second problem, as pointed out by Maier [7], is that there can be different transport coefficients parallel vs. perpendicular to the grain boundaries. Finally, space charge regions result in spatially varying electrical properties, which are not accounted for in two-phase composite models.

The modeling of conventional, microcrystalline electroceramics is based on the pioneering work of Bauerle [8], who developed an equivalent circuit representation for conductive ceramics with resistive grain

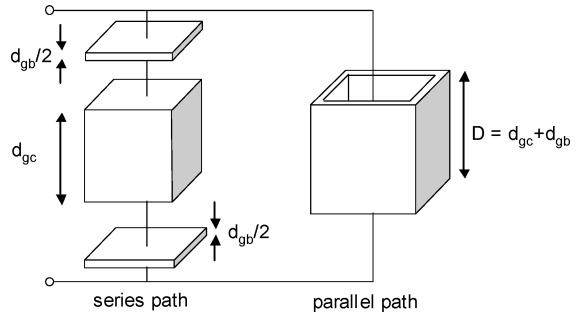

Fig. 1. Schematic representation of the brick-layer model (BLM). The unit is separated into an outer grain boundary path in parallel with a serial path of grain core and capping grain boundary.

boundaries. Beekmans and Heyne [9] conceived a simple boundary layer model, later labeled the "brick-layer model" by Burggraaf and co-workers [10, 11]. Figure 1 shows the microstructural representation. The brick-layer model (BLM) is composed of a 3D array of cubic grain cores (bricks) arranged on a simple cubic lattice separated by homogeneous grain boundary layers. The unit cell is comprised of an outer square pipe of grain boundary material enclosing a parallelepiped containing a grain core and two grain boundary caps. The simplest form of the brick-layer model, which we refer to as the series-BLM (S-BLM), neglects the contribution of the outer parallel path and considers only the serial connections of grain core and capping grain boundary layers. The impedance response modeled by a Bauerle type equivalent circuit consists of two parallel resistor-capacitor (*RC*) networks in series, shown in Fig. 2(a), where the open box represents the equivalent

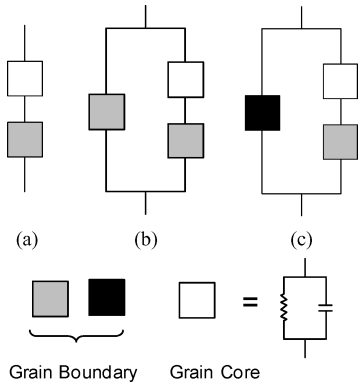

Fig. 2. Equivalent circuit representations for (a) the series brick-layer model (S-BLM), (b) the series/parallel BLM (SP-BLM), and (c) the SP'-BLM with different electrical properties parallel vs. perpendicular to the grain boundary.

circuit ($R_{gc}C_{gc}$) of the grain cores and the shaded box represents the equivalent circuit ($R_{gb}C_{gb}$) of the grain boundaries. The circuit parameters (R_{gc}, C_{gc}, R_{gb}, C_{gb}) are determined by the material properties (conductivity σ and dielectric constant ε and the relative thickness of the two phases. For microcrystalline electroceramics, with thin and highly resistive grain boundaries, the S-BLM is quite appropriate, for example, in low-purity ionic conductors with a continuous glassy grain boundary phase [12].

To extend the BLM to the nanoscale regime, where the grain boundaries and grain cores become comparable in size, the side-wall contributions must be incorporated. Näfe [13] developed a series/parallel BLM (SP-BLM) by connecting the central grain core/grain boundary serial path in parallel with the side-wall grain boundary path. The corresponding equivalent circuit is shown in Fig. 2(b). We recently applied the SP-BLM to the analysis of the impedance/dielectric response of nanocrystalline ceria [14]. To allow for different electrical conductivities perpendicular vs. parallel to the grain boundary, Maier and coworkers [15, 16] developed a modified form of the SP-BLM which we refer to as the SP′-BLM, whose equivalent circuit model is shown in Fig. 2(c).

It is anticipated that the accuracy of these brick-layer derived models decreases as the grain size approaches the nanograin regime. In such a regime the grain boundary regions (due to impurity segregation and associated depletion layers) can represent a significant volume fraction of the overall microstructure. It is also anticipated that the grain morphology will change as the grain size is reduced. Recently, Lubomirsky and co-workers [17] investigated the influence of geometry on space-charge effects in nanocrystalline ceramics. They found that for small grain sizes the charge carrier distribution is inhomogeneous along the grain boundary. In this work such effects are neglected. The microstructure is divided into two regions, homogeneous grain cores surrounded by homogeneous grain boundaries.

In the SP-BLM, current is confined to flow either through the central core (series) path or the outer (parallel) path. Figure 3 compares the DC current distribution (in the shaded Y-Z plane of the inset diagram) for current flow parallel to the direction of the applied field (Z-direction) in the SP-BLM, Fig. 3(a) vs. the more realistic nested-cube model (NCM), Fig. 3(b), which will be discussed in detail in the following section. The grain core-to-grain boundary conductivity ratio (σ_{gc}/σ_{gb}) was

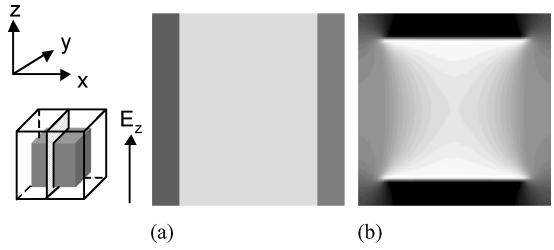

Fig. 3. Current distribution in a direction parallel to the applied electric field for a grain core to grain boundary conductivity ratio of 10, (a) SP-BLM, (b) actual current distribution (NCM). The grain core volume fraction was set at 0.31.

set at 10, and the grain core volume fraction (ϕ) was 0.31, corresponding to D/d (grain size divided by grain boundary width) of 3.09. As shown in Fig. 3(b), the current distribution for the NCM is more complicated than for the SP-BLM, with considerable current flow from the side grain boundaries toward the higher conductivity grain core. This also results in a significant decrease in the overall "composite" conductivity, as will be shown.

Motivated by the problems associated with boundary-layer models, effective medium theory (EMT) has also been used to describe the complex impedance/dielectric response of polycrystalline electroceramics. Effective medium models obviate the problems associated with restricted current paths by taking into account actual current distributions in heterogeneous media. Maxwell [18], used the idea of an effective medium to calculate the effective DC conductivity, σ_{tot}, of a two-phase composite consisting of isotropic spheres embedded randomly in a homogeneous matrix.

$$\sigma_{\text{tot}} = \sigma_1 \left\{ \frac{2\sigma_1 + \sigma_2 - 2\phi(\sigma_1 - \sigma_2)}{2\sigma_1 + \sigma_2 + \phi(\sigma_1 - \sigma_2)} \right\} \qquad (1)$$

where σ_2 is the conductivity of the dispersed spheres, σ_1 is the conductivity of the matrix, and ϕ is the volume fraction of spheres. Equation (1) assumes that neighboring spheres do not interact and is correct only to first order in volume fraction (ϕ). Beyond the dilute limit, mutual interactions between neighboring spheres become increasingly significant.

Wagner [19] later showed Eq. (1) to be valid for the complex conductivity, $\sigma^* = \sigma_{\text{DC}} + i\omega\varepsilon$. A Maxwell-Wagner (MW) medium can be visualized as built up from a space-filling array of coated spheres as in Fig. 4, with each sphere surrounded by a material containing smaller identical spheres having the mean or effective property value of the medium. As pointed out by McLachlan et al. [14], the MW model is equivalent to the upper and lower bounds for conductivity of an isotropic two-phase mixture presented by Hashin-Shtrikman [20] and the well-known Clausius-Mossoti equation for dielectrics. We henceforth refer to this model as the MW-HS model.

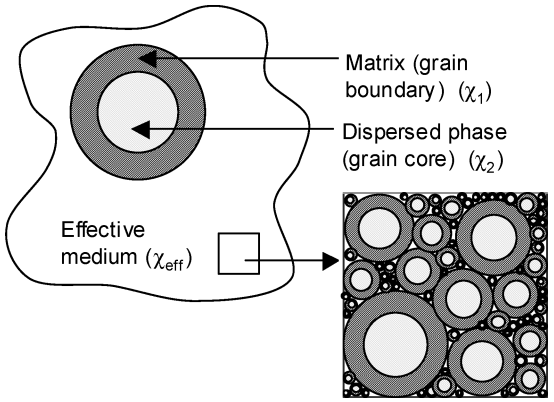

Fig. 4. Schematic of the Maxwell-Wagner (MW-HS) microstructural model.

In the low-grain boundary volume-fraction limit (thin grain boundaries), it was shown that the impedance/dielectric response of a MW-HS medium becomes indistinguishable from the brick-layer models [21]. Thin coatings, whether insulating or conductive relative to the cores, behave identically regardless of the grain morphology (i.e., spheres vs. cubic "bricks"). Furthermore, finite element analyses on "real" 2-D microstructures agreed well with BLM predictions unless grain shape became highly distorted, or a bimodal distribution of grain sizes was present [22, 23]. This means that simplified morphologies, whether spherical (i.e., the various EMT models) or cubic (e.g., the nested-cube model below), stand a very good chance of accurately describing the impedance/dielectric response of electroceramics as long as the grain structure remains reasonably monosized and equiaxed.

The present work describes the development of a 3D composite model capable of describing the AC electrical response of polycrystalline ceramics over the entire range of grain core volume fractions, from 0 (nanoscale) to 1 (microscale). One model pertinent to the present work is that of Zuzovsky and Brenner [24]. The Zuzovsky-Brenner Model (ZBM) consists of a continuous isotropic matrix phase in which is embedded a spatially periodic array of second phase

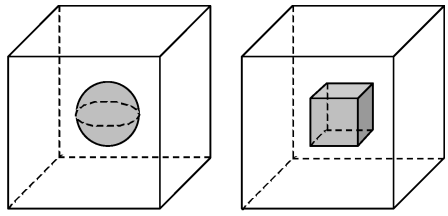

Fig. 5. Unit cells of the Zuzovsky-Brenner model (ZBM), with spherical second phase particles (grain cores) on a simple cubic lattice and (b) the nested-cube model (NCM), with cubic second phase particles (grain cores) on a simple cubic lattice.

spherical particles. The second phase can be arranged on three types of cubic lattices—face-centered cubic, body-centered cubic, and simple cubic, the unit cell of which is shown in Fig. 5(a). This model is perhaps the most representative of the situation in nanoceramics with relatively thick grain boundary layers; grain core morphology will most likely *not* retain overall grain shape due to smearing/rounding of boundary layers (e.g., space charge regions). The problem with the ZBM is that a percolation threshold (grain core-to-grain core contact) is reached at a grain core volume fraction of 0.52 for a simple cubic lattice.

The development of an analogous nested-cube model (NCM) is presented in this work, the unit cell of which is shown in Fig. 5(b). The NCM is a generalization of the BLM with its cubic morphology. However, it also considers the actual current distribution within the microstructure. It does not have a percolation threshold and is capable of describing the impedance/dielectric behavior for cubic grains over the entire range of grain core fractions. At low grain core volume fractions, it is anticipated that the NCM will differ somewhat from the MW-HS and ZBM behavior because of the difference in the basic shape of the grain core. This will be discussed in detail in the second paper. At large grain core volume fractions, however, the NCM results are expected to approach those of the boundary-layer models. When the grain boundaries are thin, the NCM and the brick-layer models should be microstructurally and electrically indistinguishable.

2. Details of the Numerical Model

The NCM is not tractable analytically. Therefore, the complex conductivity has to be solved numerically. A FORTRAN-77 finite difference numerical program, named ac3d.f, was modified to perform pixel-based computer calculations at finite frequencies [25, 26]. The program was originally designed to compute the electrical properties of random materials whose microstructure can be represented by a 3-D digital image. It is assumed that each pixel of the image can be treated as a homogeneous phase of known admittance, the admittance being modeled by a parallel (RC) circuit. In the present work the computer program was used to simulate a non-random but analytically intractable geometry. To simulate the NCM, pixels were assigned to either the grain core or the grain boundary. A diagonalized complex conductivity was assigned to the two phases. A system size ranging from 20^3 to 80^3 pixels was employed to represent the 3-D structure of the NCM. In the computation process, each pixel has six orthogonal (RC) circuits extending from its center to the boundaries of the pixel. Neighboring pixels were connected by joining the two bonds together producing a three-dimensional electrical network with a finite difference node at the center of each pixel. A conjugate gradient method was then used to solve Laplace's equation at each frequency to give the complex conductivity of the microstructure. Real and imaginary conductivities were then converted to impedance and modulus quantities using standard equations.

To generate the periodic simple cubic lattice of the NCM, it was necessary to add a shell of imaginary states around the central grain and grain boundaries to maintain periodic boundary conditions [25, 26]. For a given grain core volume fraction, the system size was varied to assess the effect of spatial resolution [27]. A plot of conductivity versus $1/N$ (where N is the number of pixels) was extrapolated to give the conductivity at $1/N \rightarrow 0$. The computational uncertainty associated with the NCM, due to the use of the $1/N$ extrapolation is less than one percent, which is very small. The program was able to compute the voltage at each pixel allowing the calculation of all the local currents within the microstructure as well as the total current within the sample.

Analytical equations exist for the resistance/conductance of the other models considered, which could therefore be evaluated in terms of complex conductivities. The same standard equations were employed in each case to obtain to impedance and modulus formats. Equations for impedance and modulus formats are given in the Appendix. We also considered Bode plots (log-log plots of

real and imaginary impedance or capacitance vs. frequency).

3. Results and Discussion

The NCM was initially used to study the two extremes of low grain core volume fraction and very high grain core volume fraction. In the first case, due to widely dispersed grain cores in a continuous grain boundary matrix, close agreement with the effective medium models (MW-HS, ZBM) is anticipated. In the second case, due to thin grain boundary layers, it is reasonable to expect good agreement with the brick-layer models (S-BLM, SP-BLM).

Figure 6(a) shows an impedance or Nyquist plot (Z-plane) and Fig. 6(b) a modulus (M-plane) plot for NCM, ZBM, and MW-HS model results, for a low grain core volume fraction, $\phi = 0.048$, corresponding to D/d (grain size divided by grain boundary width) of 1.57. The ratio of grain-core-to-grain-boundary properties were set at $(\sigma_{gc}/\sigma_{gb}) = 10$ and $(\varepsilon_{gc}/\varepsilon_{gb}) = 0.1$. In the low grain core volume fraction limit (thick grain boundaries), there is good agreement between the ZBM, the NCM and the MW-HS model; they all converge to the exact impedance/dielectric response of the MW-HS model in the dilute limit.

In the high grain core volume fraction limit (thin grain boundaries), there is good agreement between the NCM and the brick-layer models. This is illustrated in Fig. 7(a) (Nyquist plot) and 7(b) (Modulus plot), where NCM and SP-BLM results are virtually indistinguishable. For these simulations, the grain core-to-grain boundary conductivity ratio was set at $(\sigma_{gc}/\sigma_{gb}) = 10$, and their dielectric constants were assumed to be identical ($\varepsilon_{gc} = \varepsilon_{gb}$). The grain core volume fraction was $\phi = 0.927$, corresponding to D/d (grain size divided by grain boundary width) of 40. Again, there is excellent agreement with the MW-HS model.

Significant differences between the NCM and the BLM's occur at intermediate grain core volume fractions. Figures 8(a) and (b) show Z-plane and M-plane plots, respectively, for a conductivity ratio of 10 $(\sigma_{gc}/\sigma_{gb})$ and a dielectric constant ratio of 1 $(\varepsilon_{gb} = \varepsilon_{gc})$. The grain core volume fraction was set at 0.385. This corresponds to D/d (grain size divided by grain boundary width) of approximately 3.7. There is reasonable agreement between the NCM and the MW-HS predictions; however, the SP-BLM results are noticeably shifted in both Nyquist and Modulus plots. For example, from Fig. 8(a) the DC resistance determined from the NCM and MW-HS agree to within 3% whereas the SP-BLM overestimates the resistance by 10%. This is due to the unrealistic current flow in the SP-BLM, i.e., restricted to central (serial) or outer (parallel) paths of the SP-BLM (see Fig. 1). In contrast, both the NCM and the MW-HS effective medium model allow for more realistic current distributions.

To test the general validity of the various models, we calculated the DC conductivity vs. grain core volume fraction over the entire range of values ($0 < \phi < 1$) for conductivity ratios of $\sigma_{gc}/\sigma_{gb} = 10$ (conductive

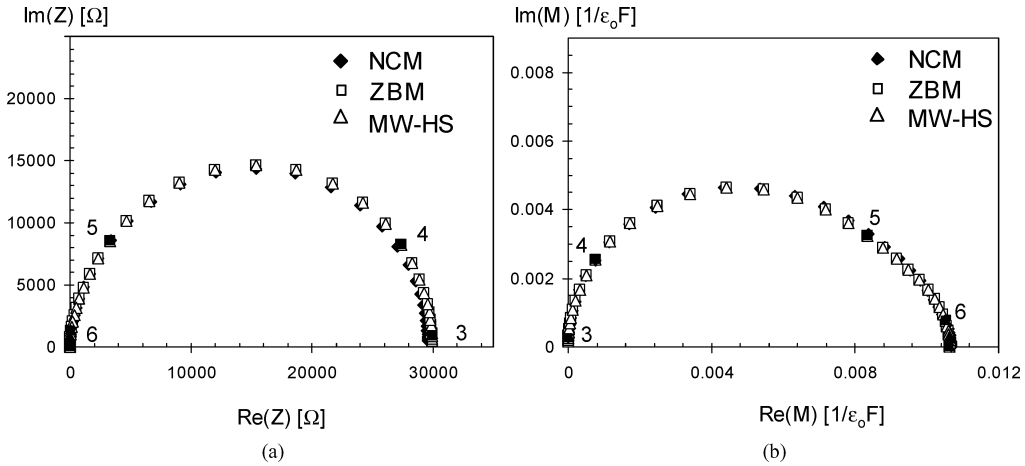

Fig. 6. Simulated (a) impedance and (b) modulus response for various models assuming $\sigma_{gc}/\sigma_{gb} = 10$ and $\varepsilon_{gc}/\varepsilon_{gb} = 0.1$ and a grain core volume fraction of 0.048, with log(frequency) markers as shown.

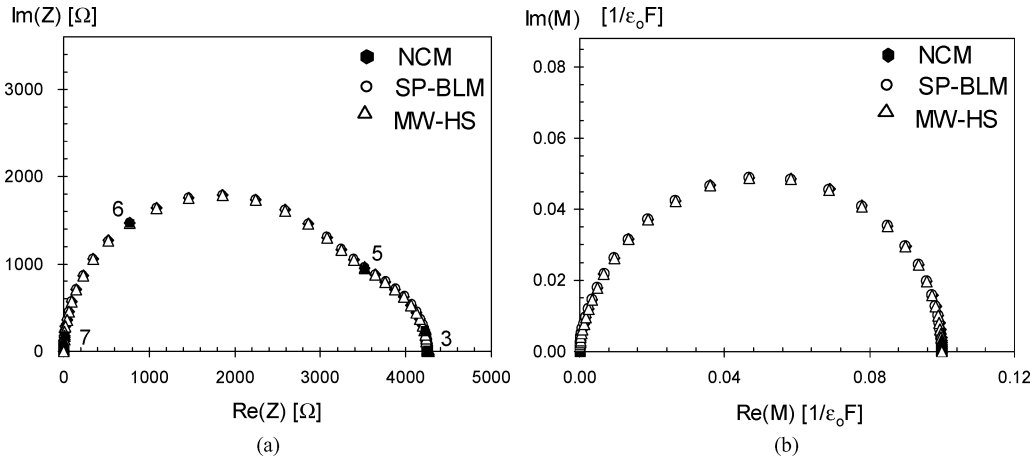

Fig. 7. Simulated (a) impedance and (b) modulus response for various models assuming $\sigma_{gc}/\sigma_{gb} = 10$ and $\varepsilon_{gc}/\varepsilon_{gb} = 1$ and a grain core volume fraction of 0.927, with log(frequency) markers as shown.

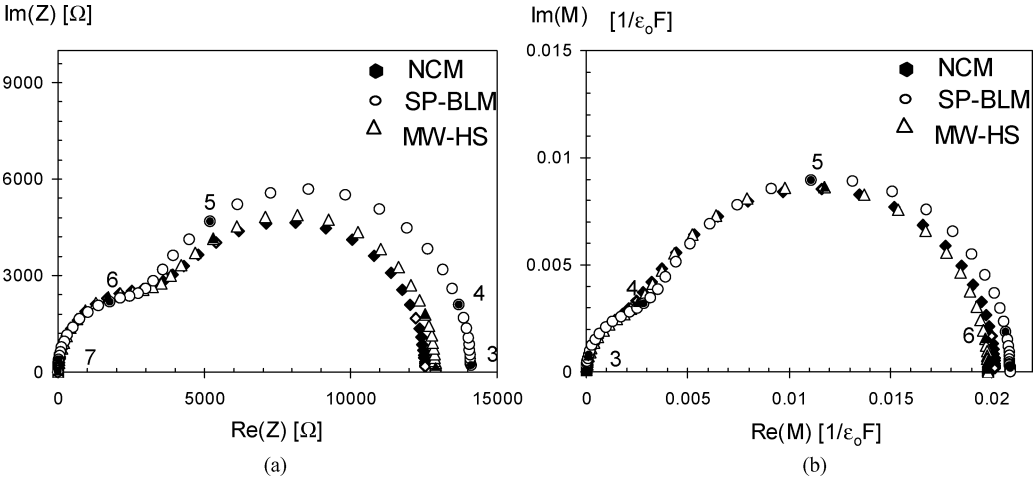

Fig. 8. Simulated (a) impedance and (b) modulus response for various models assuming $\sigma_{gc}/\sigma_{gb} = 10$ and $\varepsilon_{gc}/\varepsilon_{gb} = 1$ and a grain core volume fraction of 0.385, with log(frequency) markers as shown.

grain cores) and $\sigma_{gc}/\sigma_{gb} = 0.1$ (resistive grain cores). It should be stressed that the MW-HS model represents the upper and lower limits for isotropic two-phase composites. Whenever model predictions fall outside the region bounded by the two MW-HS lines, such predictions are invalid (not physically reasonable). Figure 9(a) compares the S-BLM and ZBM with the MW-HS model. The ZBM is in good agreement with the MW-HS model for all grain core fractions up to its percolation threshold ($\phi = 0.52$), as expected for the conductivity ratios of $\sigma_{gc}/\sigma_{gb} = 10$ and $\sigma_{gc}/\sigma_{gb} = 0.1$. Beyond the percolation threshold, the ZBM is no longer valid. The S-BLM is in good agreement with the MW-HS at high grain core fractions, as anticipated, but deviates markedly at small grain core fractions. This is due to ignoring side-wall contributions (see Fig. 1) and the correspondingly unrealistic current distribution.

Figure 9(b) shows SP-BLM predictions vs. the MW-HS model as a function of grain core volume fraction. In the thin grain boundary limit, there is good agreement between the two models. At intermediate grain core volume fractions, however, there are noticeable differences between the two models. As was pointed out by McLachlan et al. [21], the SP-BLM results

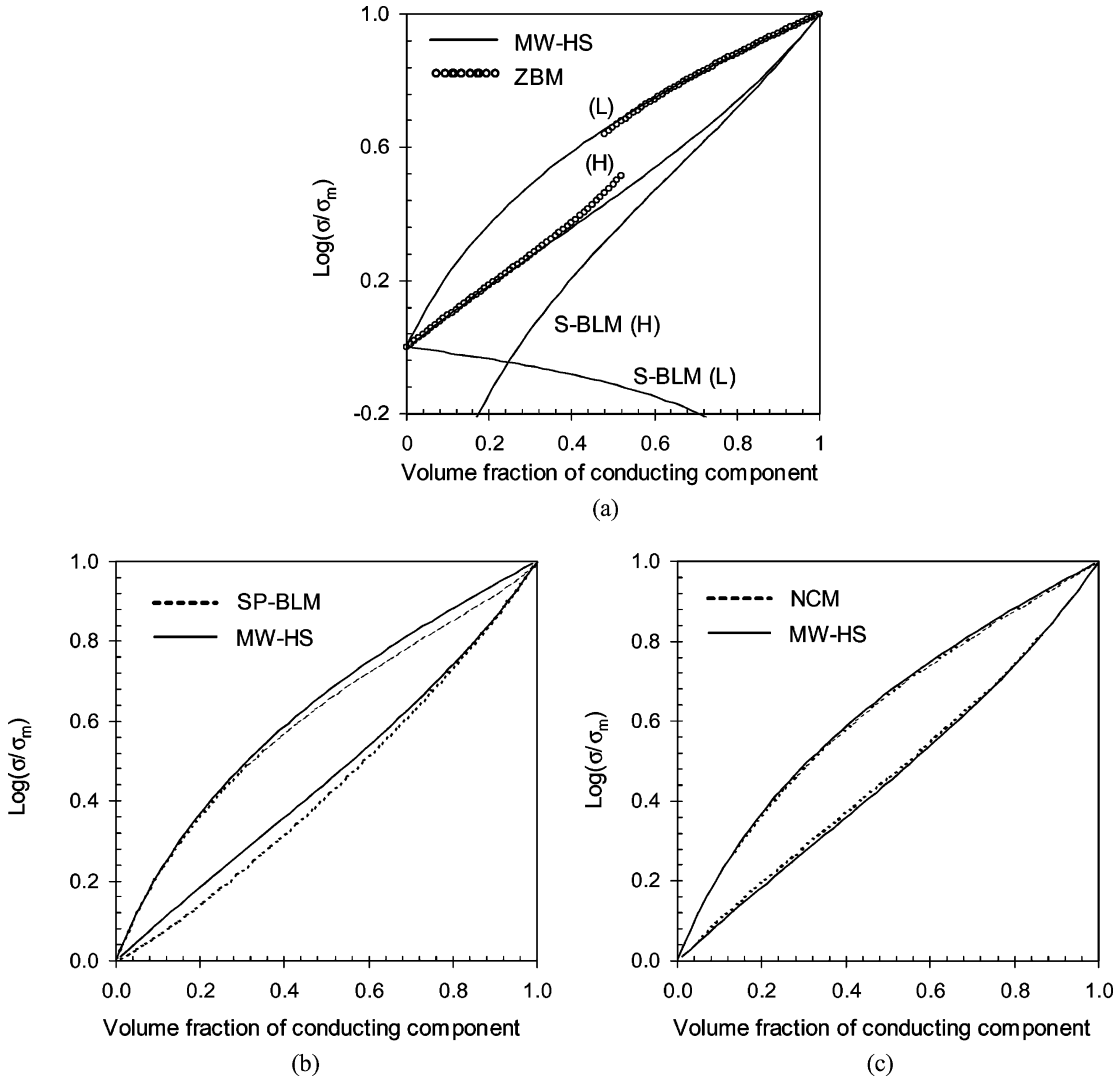

Fig. 9. DC conductivity bounds for various models assuming $\sigma_{gc}/\sigma_{gb} = 10$ for the lower bound and $\sigma_{gb}/\sigma_{gc} = 10$ for the upper bound. In (a) H-represents $\sigma_{gc}/\sigma_{gb} = 10$ and L-$\sigma_{gb}/\sigma_{gc} = 10$.

(conductive grain cores) tend to lie outside the allowed range for isotropic two-phase composites, and are physically unrealistic.

In contrast to the other models, the NCM is in close agreement with the MW-HS model over the entire range of grain core volume fractions, for both conductive and resistive grain cores. This is seen in Fig. 9(c). Furthermore, at all volume fractions, the NCM results consistently fall within the allowed (physically reasonable) range bounded by MW-HS upper and lower curves.

In summary, the nested cube model has the following characteristics:

(1) The NCM closely matches brick-layer model predictions (S-BLM, SP-BLM) at large grain core volume fractions (thin grain boundaries).
(2) The NCM approaches effective medium model predictions (e.g., ZBM) at small grain core volume fractions (thick grain boundaries).
(3) The NCM results lie within the allowed MW-HS upper and lower bounds over the entire range of grain core volume fractions.

(4) The NCM closely follows MW-HS behavior over the entire range of grain core volume fractions.

The effectiveness of the NCM lies in its ability to describe two-phase composite behavior over the entire range of volume fractions. There is no percolation threshold (as for the ZBM) and actual current distributions are taken into account (vis-à-vis the S-BLM and SP-BLM). However, the NCM has two potential drawbacks. First, it is computationally intensive. Second, it is certainly *not* an accurate representation of actual electroceramic microstructure. This may not be a problem at large grain core volume fractions (thin grain boundaries), as argued above, but shape effects must be considered at other grain core volume fractions (e.g., cubes vs. spheres vs. dodecahedra). For very small grain core volume fractions it is unlikely that the grain core and grain boundary regions are homogeneous, the transition region over which the electrical properties change is likely to be significant and has not been considered in the above analysis.

In Part 2 we consider grain core shape effects on electrocomposite behavior and further explore the close agreement between the NCM and the MW-HS effective-medium model. We also consider a wider range of electrical properties (e.g., conductivity). For practical purposes, we develop a closed-form solution for deriving component electrical properties (grain core vs. grain boundary) from experimental impedance data.

4. Conclusions

A pixel-based finite-difference "nested cube model" was developed to investigate the validity of existing two-phase electrocomposite models for polycrystalline ceramics. The NCM is capable of describing the impedance/dielectric behavior of electroceramics over the entire range of grain core volume fractions, from the nanocrystalline regime (where grain cores are small) to the microcrystalline regime (where grain boundaries are thin). It agrees well with effective medium theories in the small grain core limit (e.g., the Zuzovsky-Brenner model, ZBM) and with grain boundary-layer models in the large grain core limit (e.g., the series and series/parallel brick-layer models, S-BLM, SP-BLM). As opposed to the ZBM, which exhibits a percolation threshold at grain core volume fraction $\phi = 0.52$, there is no percolation threshold for the NCM. In contradistinction to the S-BLM and SP-BLM, which exhibit physically unreasonable conductivities at intermediate grain core fractions (with values lying outside the Hashin-Shtrikman bounds), NCM values fall within the MW-HS bounds at all grain core volume fractions.

Part 2 of this series explores the close agreement between the NCM and MW-HS effective medium theory over the entire range of grain core volume fractions, and develops a closed-form equation for extracting component electrical properties from experimental impedance data.

Appendix

The complex conductivity σ^* obtained as a function of angular frequency (ω) and grain core volume fraction (ϕ) was converted to the impedance and modulus using the following equations.

$$Z_{\mathrm{mr}} = GF\left(\sigma_{\mathrm{mr}}/\left(\sigma_{\mathrm{mr}}^2 + \sigma_{\mathrm{mi}}^2\right)\right) \tag{A.1}$$

$$Z_{\mathrm{mi}} = -GF\left(\sigma_{\mathrm{mi}}/\left(\sigma_{\mathrm{mr}}^2 + \sigma_{\mathrm{mi}}^2\right)\right) \tag{A.2}$$

$$M_{\mathrm{mr}} = -\omega Z_{\mathrm{mi}} \tag{A.3}$$

$$M_{\mathrm{mi}} = \omega Z_{\mathrm{mr}} \tag{A.4}$$

Here, *GF* is a geometric factor used to convert from conductivity to conductance.

Acknowledgments

This work was supported in part by the U.S. Department of Energy under grant no. DE-FG02-84ER45097 and in part by the National Science Foundation under grant no. DMR-0076097 through the Materials Research Science and Engineering Center program.

References

1. J.T. Irvine, D.C. Sinclair, and A.R. West, *Adv. Mater.*, **2**(3), 132 (1990).
2. B.-S. Hong, S.J. Ford, and T.O. Mason, *Key Engineering Materials*, **125/126**, 163 (1997).
3. D.C. Sinclair and A.R. West, *J. Appl. Phys.*, **66**(8), 3850 (1989).
4. Y.-M. Chiang, E.B. Lavik, I. Kosacki, H.L. Tuller, and J.Y. Ying, *Appl. Phys. Lett.*, **69**, 185 (1996).
5. Y.-M. Chiang, *J. Electroceram.*, **1**(3), 205 (1997).
6. H.L. Tuller, *Solid State Ionics*, **131**, 143 (2000).
7. J. Maier, *Ber. Busenges. Phys. Chem.*, **90**, 26 (1986).
8. J.E. Bauerle, *J. Phys. Chem. Solids*, **30**, 2657 (1969).
9. N.M. Beekmans and L. Heyne, *Electrochim. Acta*, **21**, 303 (1976).

10. T. van Dijk and A.J. Burggraaf, *Phys. Stat. Solidi A*, **63**, 229 (1981).
11. M.J. Verkerk, B.J. Middlehuis, and A.J. Burggraaf, *Solid State Ionics*, **6**, 159 (1982).
12. N. Bonanos, B.C.H. Steele, E.P. Butler, W.B. Johnson, W.B. Johnson, W.L. Worrell, D.D. Macdonald, and M.C.H. McKubre, in *Impedance Spectroscopy: Emphasizing Solid Materials and Systems*, edited by J.R. Macdonald (Wiley and Sons, New York 1987), p. 191.
13. H. Näfe, *Solid State Ionics*, **13**, 255 (1984).
14. J.-H. Hwang, D.S. McLachlan, and T.O. Mason, *J. Electroceram.*, **3**(1), 7 (1999).
15. J. Maier, *Prog. Solid State Chem.*, **23**, 171 (1995).
16. S. Kim and J. Maier, *J. Electrochem. Soc.*, **149**(10), J73 (2002).
17. I. Lubomirsky, J. Fleig, and J. Maier, *J. Appl. Phys.*, **92**(11), 6819 (2002).
18. J.C. Maxwell, *A Treatise on Electricity and Magnetism* (Clarendon Press, Oxford 1881).
19. K.M. Wagner, in Arkiv Electrotechnik, edited by H. Schering (Springer-Verlag, Berlin, 1914).
20. Z. Hashin and S. Shtrikman, *J. Appl. Phys.*, **33**, 3125 (1962).
21. D.S. McLachlan, J.-H Hwang, and T.O.Mason, *J. Electrocerm.*, **5**(1), 37 (2000).
22. J. Fleig and J. Maier, *J. Electrochem. Soc.*, **145**, 2081 (1998).
23. R. Hagenbeck and R. Waser, *Ber. Busenges. Phys. Chem.*, **101**, 1238 (1997).
24. M. Zuzovsky and H. Brenner, *J. Appl. Math. Phys.*, **28**, 979 (1977).
25. E.J. Garboczi, *NIST Internal Report*, **6269** (1998). Also available at http://ciks.cbt.nist.gov/monograph/, Chap. 2.
26. R.B. Bohn and E.J. Garboczi, *NIST Internal Report*, **6997** (2003).
27. A.P. Roberts and E.J. Garboczi, *J. Am. Ceram. Soc.*, **83**, 3041 (2000).